https://doi.org/10.5194/gmd-2023-193
Preprint. Discussion started: 5 October 2023

Geoscientific Model Development
Discussions
Open Access
EGU

Global variable-resolution simulations of extreme precipitation over Henan, China in 2021

Zijun Liu[1], Li Dong[1,2], Huiling Yuan[3], Xingrong Li[4], Dongmei Meng[5], Xiaobin Qiu[6], Dingyuan Liang[7], and Yafei Wang[8]

[1]Department of Earth and Space Sciences, Southern University of Science and Technology, Shenzhen, Guangdong, China
[2]Academy for Advanced Interdisciplinary Studies, Southern University of Science and Technology, Shenzhen, Guangdong, China
[3]School of Atmospheric Sciences; Key Laboratory of Mesoscale Severe Weather/Ministry of Education, Nanjing University, Nanjing, Jiangsu, China
[4]Shenzhen National Climate Observatory, Shenzhen, Guangdong, China
[5]Tianjin Meteorological Bureau, Tianjin, China
[6]Tianjin Key Laboratory for Oceanic Meteorology, Tianjin Institute of Meteorological Science, Tianjin, China
[7]Division of Environment and Sustainability, The Hong Kong University of Science and Technology, Hong Kong, China
[8]The Institute of Atmospheric Physics, Chinese Academy of Sciences, Beijing, China

Correspondence: Li Dong, dongl@sustech.edu.cn

Abstract. A historic rainstorm occurred over Henan, China in July 2021 ("7.20" extreme precipitation event), resulting in significant human casualties and socio-economic losses. A global variable-resolution model (MPAS-Atmosphere v7.3) was employed to simulate this extreme precipitation event, by bridging the hydrostatic and non-hydrostatic scales together. A series of simulations have been done at both quasi-uniform (60km and 15km) and variable-resolution meshes (60-15km and 60-3km). For the 48-hour peak precipitation duration (07/20-07/22), the 60-3km variable-resolution simulation coupled with the scale-aware convection-permitting parameterization scheme suite stands out predominately among other simulation experiments as it reproduces this extreme precipitation event most accurately, in terms of both the intensity and location of the peak precipitation. At 15-km resolution, the 60-15km variable-resolution simulation achieves comparable forecasting skills as the 15-km quasi-uniform simulation, but at a much reduced computing cost. In addition, at 15-km resolution, we found that the default mesoscale suite generally outperforms the convection-permitting suite at 15-km resolution as simulations coupled with convection-permitting suite missed the 3rd peak of this extreme precipitation event while the mesoscale suite did not. This implies that, when the resolution of the refined region is coarser than the cloud-resolving scale, the convection-permitting parameterization scheme suite does not necessarily work better than the default mesoscale suite, but once the refined mesh is close to the cloud-resolving scale, the convection-permitting suite becomes scale aware such that it can intelligently distinguish the convective precipitation and grid-scale precipitation, respectively. Finally, it is found that the large-scale wind field plays a vital role in affecting extreme precipitation simulations since it primarily influences the transport of the water vapor flux thereby altering the prediction of the precise peak precipitation location.

https://doi.org/10.5194/gmd-2023-193
Preprint. Discussion started: 5 October 2023

Geoscientific Model Development Discussions

1 Introduction

From July 17 to 22, 2021, a historic rainstorm occurred in Henan province of China ("7.20" extreme precipitation event), with a maximum hourly precipitation of 201.9mm. This rainstorm caused devastating urban flooding in Henan, resulting in 292 fatalities, 47 missing persons, and a direct economic loss of 53.2 billion yuan (Jinfang et al., 2021). The rainstorm event occurred under the atmospheric circulation background of the abnormally enhanced western Pacific subtropical high (WPSH), which is displaced northward as well, and the dual typhoon presence (Typhoon Infa and Cempaka) (Xu et al., 2022). The main sources of water vapor for the present heavy rain event can be attributed to three factors: the WPSH, Typhoons In-fa and Cempaka (Nie and Sun, 2022). East China frequently experiences summer extreme precipitation event such as the "7.20" event studied here due to East Asian Monsoon, tropical cyclones and mesoscale convective vortex (Ding and Johnny CL, 2005; Lonfat et al., 2004; Houze Jr, 2004). Previous studies have proposed numerous mechanisms for the occurrence and development of extreme precipitation events in eastern China. The subtropical high over the northwest Pacific is a key system affecting the East Asian summer monsoon and typhoons in the northwest Pacific region, which provides a possibility for seasonal prediction of the East Asian summer monsoon(Wang et al., 2013). The record-breaking Meiyu in the Yangtze River Basin in 2020 was characterized by a wide meridional rain belt with abundant precipitation and high frequency of occurrence of heavy rain. In addition, this long-lasting Meiyu season of 2020 is distinguished by an extended duration with an early onset and late retreat(Ding et al., 2021). Liu et al. (2020) pointed out that the summer extreme precipitation events are resulted from the sequential warm and cold Meiyu front that are regulated by the North Atlantic Oscillation. In addition, the synoptic-system-related low-level jet (SLLJ) and boundary layer jet (BLJ) are closely related to heavy precipitation events in the coastal region of South China, and the interaction between these two jets has a critical impact on convective activity initiation (Du and Chen, 2019; Zhang and Meng, 2019). Zheng and Wang (2021) investigated the influence of the three main oceans on extreme precipitation in the Yangtze River Basin and found that sea surface temperature anomalies (SSTA) in the western North Atlantic in May could effectively predict precipitation anomalies in the Yangtze River Basin in June. With the global warming trend, the occurrence of the frequency of summer extreme precipitation events is on the rise and accurately predicting the duration and location of extreme precipitation events remains a significant challenge (Sun et al., 2016). Despite numerous studies have been done related to extreme precipitation simulations and rainfall data analysis, the forecasting performance for extreme precipitation events like the "7.20" rainstorm remains unsatisfactory, highlighting the need for improving the forecasting model to achieve sufficient prediction skills. (Chen et al., 2020; Sun et al., 2018; Liu et al., 2020).

The Model for Prediction Across Scales (MPAS-Atmosphere) is an advanced atmospheric forecasting model that has been widely applied to predict heavy rainfall, in particular, with the variable-resolution feature. Zhao et al. (2019) conducted MPAS experiments on the 2012 heavy rainfall event associated with Meiyu front in East Asia and pointed out that the model resolution has a significant impact on the strength and location of updrafts and precipitation. Additionally, Zhao et al. (2019) found that the convection-permitting Scheme is also suitable for global variable-resolution simulations. Xu et al. (2021) found that the low-resolution (60km) MPAS simulation overestimated the precipitation frequency (PF) of the Meiyu front precipitation, while underestimating the precipitation amount (PA) and intensity (PI), while, in contrast, the high-resolution (4km)

MPAS simulation captured the diurnal cycle of PA well, even in the absence of typhoon influence. Furthermore, Cheng et al. (2023) compared MPAS global variable-resolution (MPAS-VR) with MPAS regional configuration (MPAS-RCM) and found that MPAS-VR outperformed MPAS-RCM in capturing the mean climate state, interannual variability, and extreme events of the East Asian summer monsoon. Moreover, the comparison between MPAS-VR and MPAS-RCM indicates that the former is a promising option for regional climate simulations as it can capture regional climate features with higher fidelity. These findings suggest that MPAS has the potential to provide more accurate predictions of heavy rainfall, especially with the global variable-resolution capability. The results also demonstrate the importance of selecting appropriate model resolution and parameterization scheme when predicting precipitation events.

To date, there has been relatively little work conducted on the simulation of extreme precipitation events in eastern China with the global variable-resolution MPAS model. This is a crucial research gap that needs to be filled as extreme precipitation events can have devastating consequences, leading to flash floods, landslides, and other severe weather-related disasters (Li et al., 2016; Zhai et al., 2005; Ding et al., 2008). Therefore, it is imperative to further investigate the performance of MPAS in simulating extreme precipitation events. This can be achieved through the analysis of its spatial and temporal resolution, parameterizations, and initialization methods (Liang et al., 2021; Zhao et al., 2016; Rauscher et al., 2013; Davis et al., 2016; Wang, 2022; Fowler et al., 2016). Furthermore, the evaluation of the performance of MPAS in simulating extreme precipitation events can help improve the accuracy and reliability of operational forecast of extreme precipitation events. In the present work, Section 2 introduces the data, MPAS model, physics parameterizations, and experimental design. Section 3 presents the evaluation of the MPAS experiments configured with different resolutions. Section 4 further analyzes the simulation performances with different parametrization scheme suites. The findings are summarized in Section 5.

2 Data and Methods

2.1 Observed and Reanalysis Data

Hourly surface observation data at 178 stations, including precipitation, temperature at 2m, and relative humidity, are provided by the National Meteorological Information Center of CMA (https://data.cma.cn/) to evaluate the simulated record-breaking heavy rainfall event that occurred during 20–21 July 2021 over Henan, China (32–37°N, 110–118°E). The hourly precipitation and wind field dataset from the European Centre for Medium-Range Weather Forecasts (ECMWF) Reanalysis (ERA5, 0.25°×0.25°) is used as a reference to evaluate the simulated distributions of precipitation and winds (https://cds.climate.copernicus.eu/cdsapp#!/home). For comparison, the global forecast products starting from 00:00 UTC on 19 July 2021 at 0.25°horizontal resolutions are also utilized. All the above-mentioned data has undergone strict quality control.

2.2 MPAS-Atmosphere(MPAS-A) Model

The MPAS model (version 7.3) used in this study is a fully compressible non-hydrostatic model designed for weather and climate prediction (Skamarock et al., 2012; Skamarock and Klemp, 2008). MPAS utilizes C-grid staggering of prognostic

https://doi.org/10.5194/gmd-2023-193
Preprint. Discussion started: 5 October 2023

Geoscientific Model Development Discussions
Open Access

Table 1. Main Parameterization Schemes of MPAS

Parameterization	Mesoscale Scheme	Convection-Permitting Scheme
Convection	New Tiedtke	Grell-Freitas
Microphysics	WSM6	Thompson(non-aerosol aware)
Land surface	Noah	Noah
Boundary layer	YSU	MYNN
Surface layer	Monin-Obukhov	MYNN
Radiation, LW	RRTMG	RRTMG
Radiation, SW	RRTMG	RRTMG
Cloud fraction for radiation	Xu-Randall	Xu-Randall
Gravity wave drag by orography	YSU	YSU

variables and centroidal Voronoi meshes for sphere discretization. In MPAS, the grid refinement allows for a smooth transition from the coarse-mesh region of the globe to the fine-mesh region for the region of interest. MPAS uses the unstructured mesh based on spherical centroidal Voronoi tessellations (SCVTs), which allows the discretization of the sphere into either global quasi-uniform mesh or variable-resolution mesh. The terrain-following hybrid coordinate is used for vertical discretization (Klemp, 2011). The MPAS atmospheric dynamical core solves the fully compressible non-hydrostatic equations of motion (Klemp et al., 2007). The vertical coordinate surfaces are progressively smoothed with height to eliminate the impact of small-scale terrain structures. The dynamical solver integrates the flux-form compressible equations using the split-explicit technique (Klemp et al., 2007). The third-order Runge-Kutta scheme is used for the basic temporal discretization, along with the explicit time-splitting technique (Wicker and Skamarock, 2020), similar to that of the Weather Research and Forecasting (WRF) model (Skamarock and Klemp, 2008). The scalar transport scheme used by MPAS on its Voronoi mesh is explicated with the monotonic option used for all moist species (Skamarock and Gassmann, 2011). Extensive testing of MPAS simulations on idealized and realistic cases has verified that smooth transitions between the fine and coarse-resolution regions of the mesh do not significantly distort the atmospheric flow (Skamarock et al., 2012; Park et al., 2013).

MPAS incorporates two sets of built-in physical parameterization schemes taken from the WRF model, specifically mesoscale (MS) suite and convection-permitting (CP) suite (Table 1). The mesoscale physics suite has been tested for mesoscale resolutions (dx>10 km cell spacing) and is not appropriate for convective-scale simulations because the Tiedtke convective scheme removes convective instability before the resolved-scale motions (convective cells) can respond to it. The convection-permitting physics suite is appropriate at spatial resolutions allowing for both explicitly resolved hydrostatic and nonhydrostatic motions. It has been tested for mesh spacings from several hundred kilometers down to several km in MPAS. The Grell-Freitas convection scheme of the convection-permitting physics suite transitions from a conventional parameterization of deep convection at hydrostatic scales (dx>10 km cell spacing) to a parameterization of shallow convection at cell spacings less than 10km. This is the recommended suite for any MPAS simulations where convection-permitting meshes (dx<10km) are employed. For in-

https://doi.org/10.5194/gmd-2023-193
Preprint. Discussion started: 5 October 2023

Geoscientific Model Development Discussions
Open Access

stance, for the global variable-resolution mesh that bridges hydrostatic and non-hydrostatic scales, the Grell-Freitas convection scheme is the optimal choice.

The New Tiedtke (NTD) scheme (Zhang et al., 2011; Bechtold et al., 2004, 2008, 2014) is similar to the Tiedtke scheme (Tiedtke, 1989) used in the Regional Climate Model version4 (REGCM4) and the ECMWF model. The Grell-Freitas (GF) scheme (Grell and Freitas, 2014) is an improved Grell-Dévényi scheme (Grell and Dévényi, 2002) that attempts to extend the mesh resolution to cloud-resolving scales, as proposed by Arakawa et al. (2011). In particular, scale-aware parameterization is essential for global simulations across hydrostatic and non-hydrostatic scales. Fowler et al. (2016) implemented the GF scheme in MPAS and demonstrated that this scheme is functioned as a shallow convective scheme over the mesh refined region but a deep convection scheme over the coarse resolution region. As the horizontal resolution increases, subgrid-scale motions are resolved more accurately, leading to a decrease in the contribution of convective precipitation to the total precipitation and an increase in the contribution of grid-scale precipitation (Fowler et al., 2016). For cloud microphysics, the WRF Single-Moment 6-class (WSM6) scheme (Hong and Lim, 2006) is a one-moment prognostic parameterization with ice, snow and graupel, while the Thompson scheme (Thompson et al., 2008; Thompson and Eidhammer, 2014) includes hydrometeor species and graupel processes suitable for high-resolution simulations. Two Boundary layer schemes are available in MPAS, namely, the Yonsei University (YSU) scheme (Hong et al., 2006; Hong, 2010) and the Mellor-Yamada-Nakanishi-Niino (MYNN) scheme (Nakanishi and Niino, 2006, 2009). Other available physical parameterization schemes in MPAS include the Noah land surface scheme (Chen and Dudhia, 2001), Monin-Obukhov surface layer and Rapid Radiative Transfer Model for GCMs (RRTMG) scheme (Iacono et al., 2000).

2.3 Numerical Experiments

Several experiments have been performed using MPAS on both quasi-uniform resolution meshes and variable-resolution meshes (Table 2). All simulations have been conducted with 51 vertical levels up to 30km (Skamarock et al., 2019). Two quasi-uniform resolution meshes and two variable-resolution meshes are used in this study where the higher resolution is centered over the Henan province and covers the entirety of East Asia. The quasi-uniform mesh is characterized by a globally uniform distribution of mesh spacing, whereas the variable-resolution mesh employs a high-resolution mesh in the refined region, supplemented by a transitional zone that facilitates a seamless transition between the fine- and coarse-resolution meshes. The two quasi-uniform meshes have grid spacing of approximately 15km(U15km) and 60km(U60km), respectively. The two variable-resolution meshes feature a circular high-resolution region centered over East China. Fig. 1 shows the exact mesh size distribution of the 60-3 km variable-resolution mesh (V3km) that has a refined region with grid spacing of approximately 3 km with the mesh spacing gradually increasing through a transition zone to approximately 60 km for the rest of the globe (Fig. 1). The other variable-resolution mesh has a similar mesh structure but with a mesh spacing of 15km (V15km) over the refined region with the mesh spacing gradually increasing to 60km.

To simulate the heavy precipitation event that occurred during 20–21 July 2021 over Henan province, all the MPAS experiments were initialized at 00:00 UTC on 19 July 2021 to allow for appropriate spin-up time and the modeling results for 20–22 July 2021 are analyzed. The simulations were initialized using the analysis data at 0.25°horizontal resolution at 00:00 UTC on

https://doi.org/10.5194/gmd-2023-193
Preprint. Discussion started: 5 October 2023

Geoscientific Model Development Discussions

Table 2. Numerical experiments conducted and analyzed in this study. "MS" represents the Mesoscale scheme, while "CP" represents the convection-permitting scheme suite in Table 1. "U60km"("U15km") denotes the global quasi-uniform resolution of 60km(15km). "V15km"("V3km") represents the variable resolution with the grid spacing ranging from 60km to 15km(3km), which is confined to the area illustrated in Fig. 1.

MPAS experiments						
	U60km.MS	U15km.MS	U15km.CP	V15km.MS	V15km.CP	V3km.CP
Scheme	MS	MS	CP	MS	CP	CP
Mesh resolution	U60km	U15km	U15km	V15km	V15km	V3km

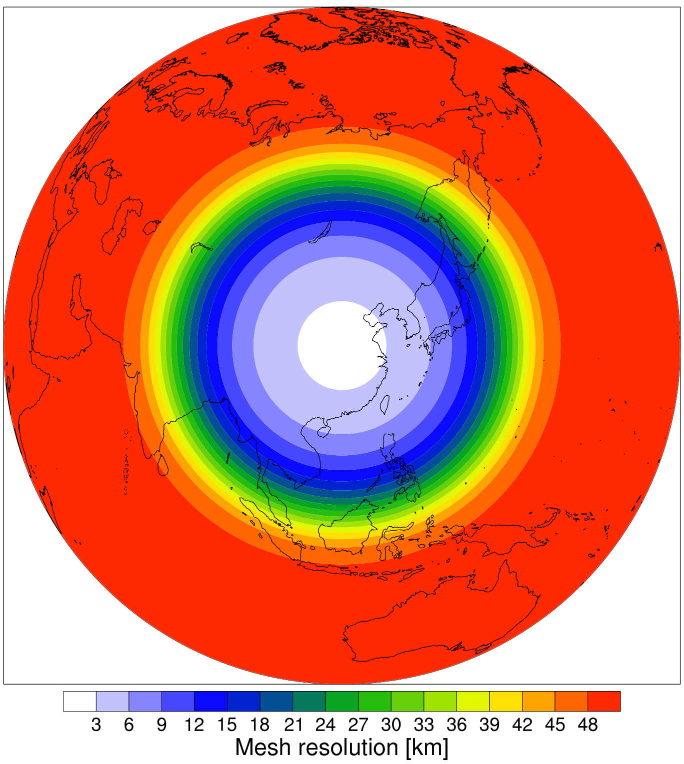

Figure 1. Global variable-resolution mesh size distribution in the 60-3km experiment

19 July 2021 from the Global Forecast System (GFS) of the National Center for Environmental Prediction (NCEP), which is the same as what is used for the GFS forecast for that period. The sea surface temperature (SST) is also prescribed the same as what is used by the GFS forecast for that period. This way, the MPAS simulations can also be compared against the GFS forecast starting from 00:00 UTC on 19 July 2021.

https://doi.org/10.5194/gmd-2023-193
Preprint. Discussion started: 5 October 2023

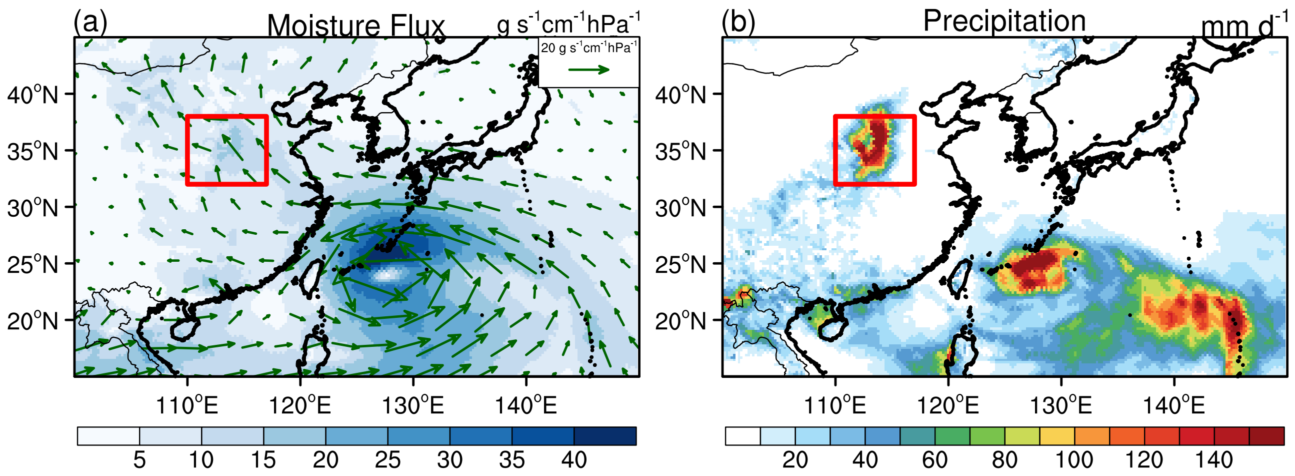

Figure 2. Background of the extreme precipitation event in Henan in July 2021. (a) Spatial distributions of moisture flux at 850-mb averaged from 00:00 UTC on July 19, 2021 to 00:00 UTC on July 23, 2021. The shading represents the intensity of water vapor flux. (b) Average daily precipitation (unit: mm/dy) from 00:00 UTC on July 19, 2021 to 00:00 UTC on July 23, 2021, derived from ERA5 hourly precipitation data. The red box denotes the target region.

3 Impacts of Resolution

Figure 2 illustrates the background of the extreme precipitation event that occurred in Henan in July 2021. Fig. 2a shows the spatial distribution of water vapor transport flux during the event, with color shading representing the intensity of water vapor transport. The region of July 21 extreme precipitation event is outlined by the red box(32°N-37°N, 110°E-120 °E). We selected July 19 to July 23 to further specify the period of interest, with a particular focus on UTC times of July 20 and July 21, as there were clear peaks during this period (Fig. 11; Fig. 12). During this time, Typhoon In-Fa and Typhoon Cempaka were associated with strong water vapor transport, transporting moisture from the western Pacific and South China Sea to northern China. In the highlighted area of Henan, a conspicuous convergence of water vapor was observed. The rainfall area during this period was generally consistent with the area of maximum water vapor transport. We are particularly interested in the precipitation distribution and peaks in the Henan province during this period.

Figure 3 shows the spatial distributions of precipitation and wind at 850-mb averaged from 20 July 00:00 to 21 July 00:00 UTC from the simulations with global uniform and variable-resolution plus two parameterization schemes. The mean precipitation from the CMA stations and ERA5 reanalysis are also shown. The initiation time of the GFS forecast product coincides with the initiation time of the MPAS experiment conducted in this study. Concentrated heavy rainfall zones are evident in the CMA observations for the central and northern regions of Zhengzhou city, Henan province. Table 3 shows the correlation coefficient of simulated and observed precipitation. The results of the model simulations are presented in Fig. 3d-i. While precipitation exceeding 150 mm d^{-1} is predicted in the Henan province, the spatial distribution of the precipitation pattern exhibits variations among the simulations. The spatial correlation coefficient of precipitation between the observation and the

https://doi.org/10.5194/gmd-2023-193
Preprint. Discussion started: 5 October 2023

Geoscientific Model Development
Discussions

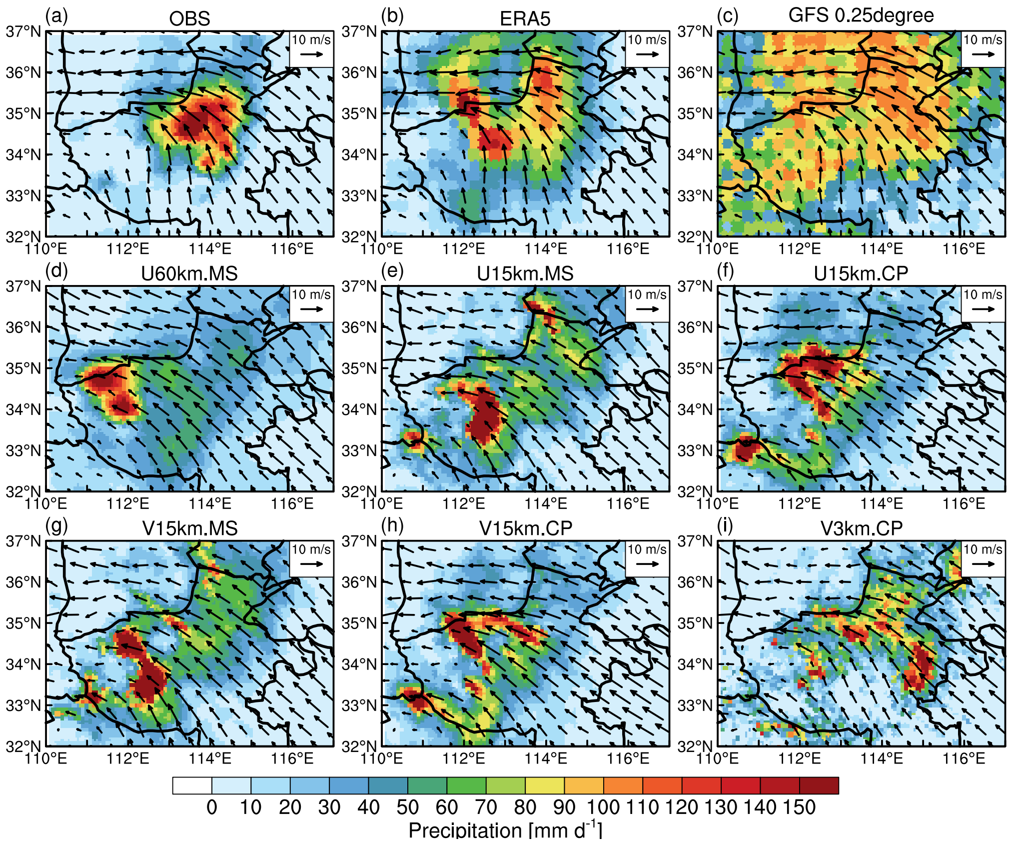

Figure 3. The observed mean precipitation from the CMA stations (a), ERA5 reanalysis (b), GFS 0.25°(c) are shown. Spatial distributions of precipitation and wind fields at 850-mb averaged from 20 July 00:00 to 21 July 00:00 UTC for the simulations with global uniform (60km, 15km) and variable (60-15km, 60-3km) resolutions, along with two parameterization schemes (MS : mesoscale scheme suite, CP : convection-permitting scheme suite) are shown in (d) through (i).

V3km.CP simulations exhibits the greatest magnitude among all model simulations with a value of 0.51. Despite having different mesh configuration, the simulated results of V15km.MS and U15km.MS are similar, as well as for the performance of V15km.CP and U15km.CP. However, U60km.MS failed to capture the heavy precipitation occurring near Zhengzhou and incorrectly predicted the precipitation by locating the maximum precipitation area to the southwest of Zhengzhou, due to the coarse grid resolution utilized in this simulation. Table 4 shows the correlation coefficients of wind at 850-mb between the various simulations and observed CMA data. The correlation coefficient of simulated and observed precipitation is in good agreement with the correlation coefficient of the simulated and observed wind at 850-mb, indicating a coherent response of precipitation to the atmospheric wind field. Interestingly, the observed maximum precipitation location is coincident with the apparent curving of the 850-mb wind vector, namely, the wind changes from southerly to southeasterly and then easterly, based on Fig. 3a. However, all simulations seem to fail to precisely reproduce the sharp curving of the horizontal wind, namely,

https://doi.org/10.5194/gmd-2023-193
Preprint. Discussion started: 5 October 2023

Table 3. The correlation coefficients of precipitation between the various simulations and observed CMA data are listed below. The bold font in the table denotes statistical significance at the 95% confidence level. "20 July precipitation pattern" corresponds to the correlation coefficiens between the simulations and OBS from 20 July 00:00 to 21 July 00:00 UTC of precipitation (Fig. 3). Similarly, "20 July Precipitation-Lon" represents the correlation coefficient of Fig. 5, while "21 July precipitation pattern" represents Fig. 6, "21 July Precipitation-Lon" represents Fig. 8, "Latitude-Time" represents Fig. 11, and "Longitude-Time" represents Fig. 12.

Correlation Coefficints	U60km.MS	U15km.MS	U15km.CP	V15km.MS	V15km.CP	V3km.CP
20 July precipitation pattern	0.31	**0.33**	**0.38**	0.31	**0.35**	**0.51**
20 July Precipitation-Lon	**0.43**	**0.78**	**0.58**	**0.71**	**0.56**	**0.86**
21 July precipitation pattern	**0.37**	**0.32**	0.07	0.28	0.06	**0.62**
21 July Precipitation-Lon	**0.63**	**0.43**	0.22	**0.51**	0.14	**0.89**
Latitude-Time (mm/hr)	**0.42**	**0.44**	**0.40**	**0.51**	**0.42**	**0.51**
Longitude-Time (mm/hr)	**0.41**	**0.51**	**0.50**	**0.50**	**0.44**	**0.58**

Table 4. The correlation coefficients of wind at 850-mb between the various simulations and observed CMA data are listed below. The bold font in the table denotes statistical significance at the 95% confidence level. "20 July U(V) component" corresponds to the correlation coefficiens between the simulations and OBS from 20 July 00:00 to 21 July 00:00 UTC of zonal(meridional) wind at 850-mb (Fig. 3). Similarly, "20 July U(V) component" corresponds to the correlation coefficiens between the simulations and OBS from 21 July 00:00 to 22 July 00:00 UTC (Fig. 6).

Correlation Coefficints	U60km.MS	U15km.MS	U15km.CP	V15km.MS	V15km.CP	V3km.CP
20 July U component	0.05	-0.10	**0.35**	-0.02	**0.38**	**0.69**
20 July V component	**0.93**	**0.89**	**0.89**	**0.86**	**0.90**	**0.93**
21 July U component	**0.29**	**0.35**	0.12	0.27	0.17	**0.40**
21 July V component	**0.53**	**0.68**	**0.43**	**0.63**	**0.46**	**0.64**

most of the simulated wind vector merely turns from southeasterly to easterly instead. Hence, the mislocation of the simulated maximum precipitation is likely attributed to errors in the low-level wind simulations.

To better illustrate the performance of simulations in terms of precipitation, Fig. 4 shows the differences between the simulations and observations averaged from 20 July 00:00 to 21 July 00:00 UTC. All simulations consistently underestimated the precipitation intensity near Zhengzhou and forecasted higher intensity in the western region of Henan incorrectly except for the V3km.CP simulation. It is worth noting that V3km.CP exhibited the least pronounced discrepancies from observation, with an underestimation of 40 mm d^{-1} near Zhengzhou. These discrepancies were also more dispersed compared to other simulations. The simulations of variable- and uniform- resolutions are generally consistent at the mesh of the same fine resolution. However, the variable-resolution approach can significantly reduce computing cost. The discrepancy of U60km.MS from observation is the most pronounced among all simulations, which is consistent with the conclusion in Fig. 3.

https://doi.org/10.5194/gmd-2023-193
Preprint. Discussion started: 5 October 2023

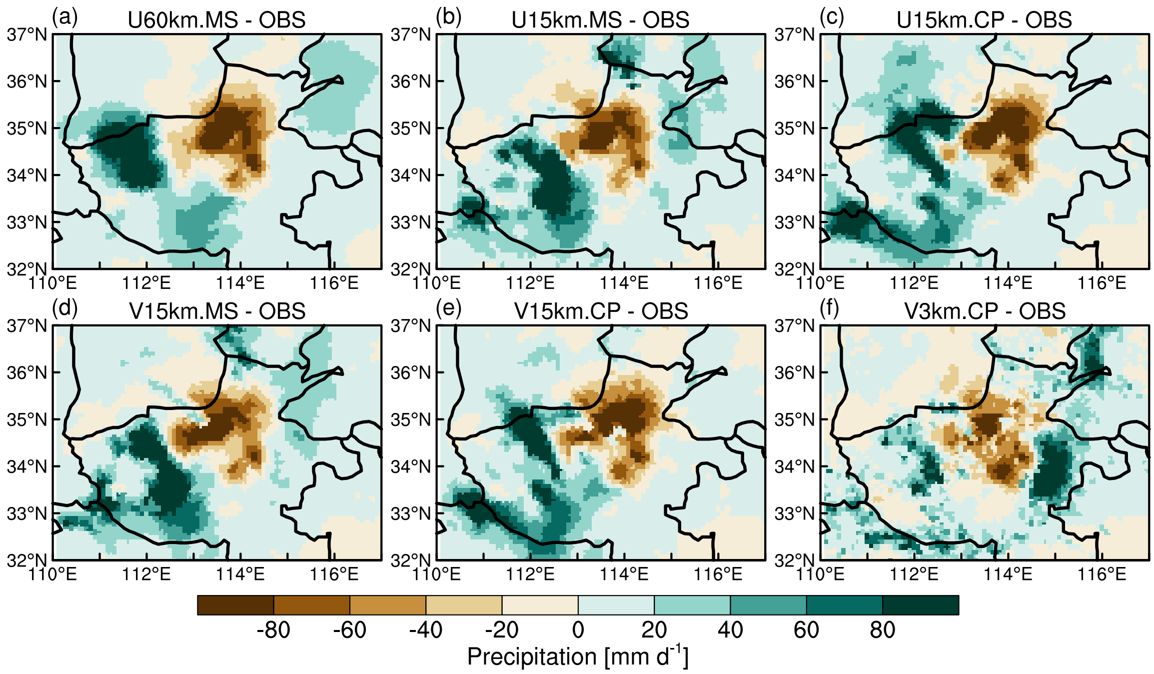

Figure 4. The difference of precipitation between CMA stations and simulations from 20 July 00:00 to 21 July 00:00 UTC.

In order to visually represent the change of observed and simulated precipitation intensity along longtitude over the peak precipitation region, we calculated the zonal distributions of precipitation averaged over the red-box region in Fig. 2 from 20 July 00:00 to 21 July 00:00 UTC as show in Fig. 5. Consistent with the previous conclusion, the V3km.CP simulation outperforms all other experimental configurations with a correlation coefficient with observations being 0.86. Regarding 15km simulations, the variable-resolution simulation generally presents a peak precipitation slightly west of that simulated by the quasi-uniform simulation. Meanwhile, for both 15km variable-resolution simulation and 15km quasi-uniform simulation, the CP parameterization suite surpasses the MS suite by presenting greater maximum precipitation close to observed values. Finally, the quasi-uniform 60km simulation presents the least sufficient performance with an excessively low simulated precipitation peak value and incorrect zonal distribution. In summary, due to the outstanding resolution and matching parameterization scheme utilized, the V3km.CP exhibits the optimal forecasting skills. On the contrary, the U60km.MS shows the worst prediction performance. The utilization of the CP scheme in the simulations effectively captures the maximum values, given the convection-permitting scheme suite is scale aware in that it can dynamically compute resolved and parameterized precipitation according to different resolutions in the variable-resolution mesh.

Figure 6 shows the comparison between observed and simulated precipitation, just same as Fig.5, except for the time period from 00UTC July 21 to 00UTC July 22. During this 24-hr period, the observed rainfall zone keeps moving northward and reaches northern Henan province indicated in Fig. 6a. Among all simulations, only V3km.CP correctly captures both the

https://doi.org/10.5194/gmd-2023-193
Preprint. Discussion started: 5 October 2023

position and intensity of the precipitation, showing a spatial correlation coefficient of 0.62 with the observations(Table 3). Generally, at 15km resolution, with the same parameterization scheme suite being selected, the variable-resolution simulation results resemble the 15km quasi-uniform simulation results closely. Meanwhile, the two sets of parameterization suites, i.e. MS vs CP, turn out to have different impacts upon the simulated precipitation at 15km resolution. Specifically, the MS parameterization suite tends to give rise to two locations of simulated peak precipitation, i.e. one is over the North Henan province, just nearly identical to the observation. The other is over the Soutwest Henan province with even greater precipitation intensity. As for the CP parameterization suite, there is nearly none precipitation simulated over North Henan province. Instead, the simulated two precipitation bands are spread out over Southwest Henan province. In this sense, the MS suite seems superior to CP for this 24-hr simulation period at 15km resolution. This can be reflected from Fig. 7 as well. However, all simulated 850-mb wind field for the second 24-hr exhibit notably inferior performance when contrasted with those of the first 24-hour simulations, specifically at the resolution of 15km(Table 4). Furthermore, Table 4 shows the U15km.CP and V15km.CP simulations of 850-mb wind field are notably inferior to those achieved with U15km.MS and V15km.MS. This discrepancy is one of the contributing factors leading to the subpar performance of the CP scheme in this 24-hr precipitation simulation. It is very likely that the simulated wind field from MS and CP parameterization suites, respectively, plays a key role in governing the location of the simulated peak precipitation. Namely, the MS suite generates prevailing 850-mb southeasterly wind which tends to maintain the peak precipitation region over North Henan province while shifting another peak precipitation region to Southwest Henan province. As for the CP suite, it seems to favor 850-mb westerly wind generation over Henan province such that the simulated peak precipitation region tends to shift further west and none peak precipitation is reproduced over North Henan province. Once again, it is confirmed that the simulated low-level wind field plays a vital role in the peak precipitation simulations, in terms of both precipitation intensity and location.

The contents presented in Fig. 8 are consistent with those in Fig. 5, but represent the hourly average precipitation from 21 July 00:00 to 22 July 00:00 UTC. The observation indicates a weakening of the precipitation peak during this period (5mm/hr), with the maximum precipitation value slightly shifting eastward to 114°E. Once again, for simulations at 15km resolution, regardless of variable-resolution or quasi-uniform mesh, it is found that the MS parameterization scheme outperforms CP scheme in terms of precipitation intensity simulation with the CP scheme predicting a precipitation intensity (3mm/hr) far below the observed value (above 5mm/hr). This is consistent with what Fig. 6 depicts. As for 3km resolution, the variable-resolution simulation with CP parameterization scheme suite achieves the supreme performance, accompanied by a pattern correlation coefficient with observations being 0.89.

4 Impacts of Parameterization

4.1 Convective Precipitation and Grid-scale Precipitation

The GF parameterization of convection utilizes a scaling factor, which is a quadratic function of the convective updraft fraction, to calculate convective and grid-scale precipitation over the coarse and refined mesh regions, respectively. To demonstrate the scale-aware performance of the GF cumulus parameterization across various resolutions, which is embedded in the convection-

https://doi.org/10.5194/gmd-2023-193
Preprint. Discussion started: 5 October 2023

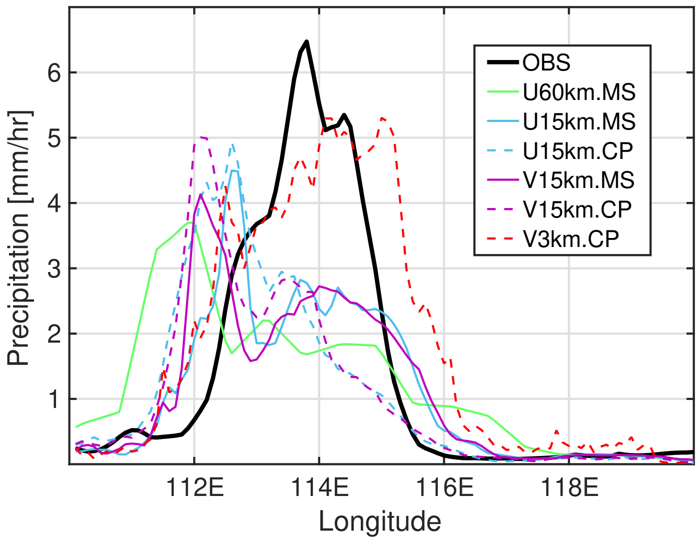

Figure 5. Zonal distributions of precipitation averaged from 20 July 00:00 to 21 July 00:00 UTC over Henan (denoted as the red box in Fig. 2) for the CMA station observations and the simulations with resolutions of 60, 15, and 3km.

permitting physics suite, we evaluate the performance of GF using quasi-uniform and variable-resolution meshes, which vary from hydrostatic (60km) to nonhydrostatic (3km) scales. Fig. 9 shows the spatial distribution of parameterized (upper four panels), resolved (medium four panels), and total (lower four panels) precipitation simulated by MPAS, averaged from 20 July 00:00 to 22 July 00:00 UTC. At the mesh resolution of 60 km, the spatial distribution of total precipitation is mainly influenced by parameterized rain, whereas the spatial maximum of precipitation is influenced by resolved rain. In contrast, at the mesh resolution of 3km, both the spatial distribution of total precipitation and the extreme precipitation are primarily influenced by resolved rain, with the impact of parameterized rain being negligible. At the mesh resolution of 15km, the contribution of parameterized rain and resolved rain to total precipitation lies between the performances of U60km.MS and V3km.CP. Furthermore, at the same resolution of 15km, the performances of mesoscale scheme suite and convection-permitting scheme suite exhibit significant differences. Specifically, the total precipitation of V15km.MS is dominated by resolved rain, which is mainly generated by cloud microphysics, while the V15km.CP is dominated by parameterized rain, which is mainly generated by convective activities. Therefore, these experiments with different parameterization schemes confirm that the GF convection parameterization scheme, utilized by the convection-permitting parameterization scheme suite, shows the scale-aware performance.

In order to show the smooth transition from coarse to fine resolution of the global variable-resolution simulation using the convection-permitting scale-aware scheme suite, we calculated the parameterized, resolved and total precipitation along with the corresponding mesh spacing in the V3km.CP simulation (Fig. 10). The comparison of the parameterized precipitation against resolved precipitation inside and outside the mesh refinement region clearly highlights the scale dependence of sim-

https://doi.org/10.5194/gmd-2023-193
Preprint. Discussion started: 5 October 2023

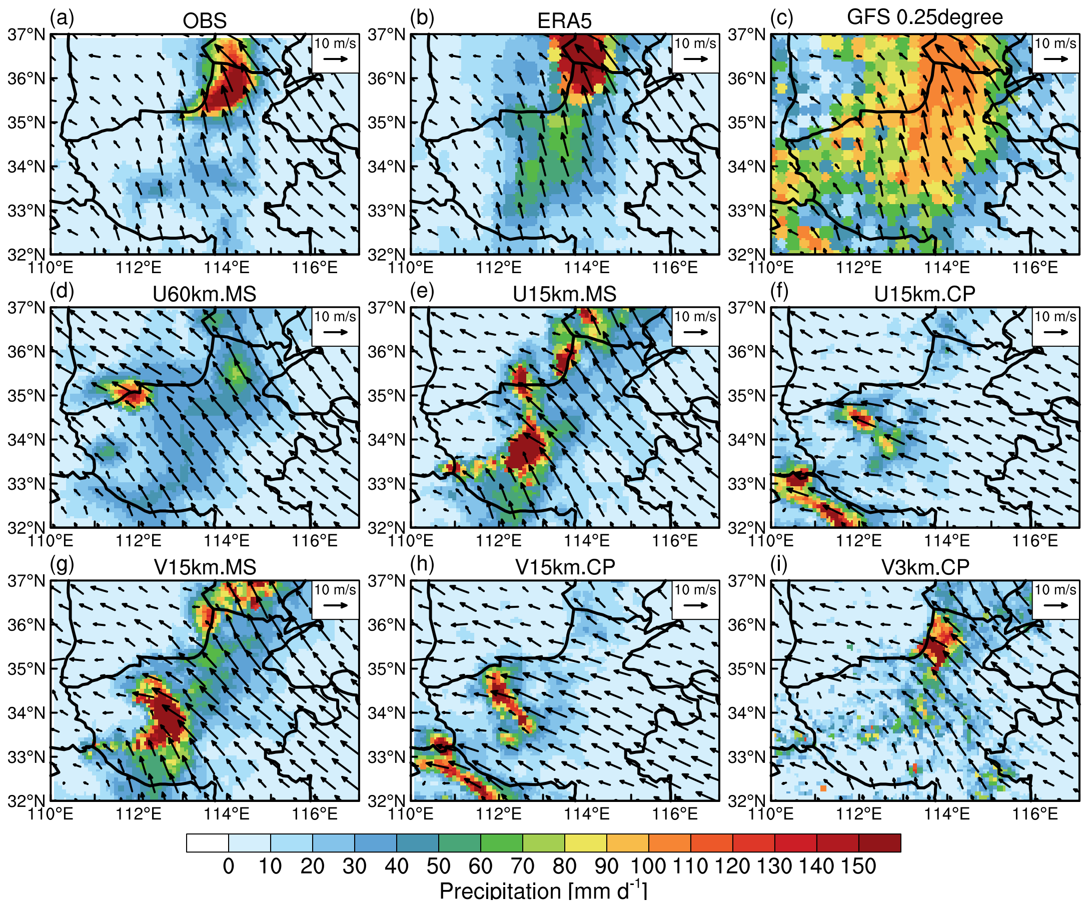

Figure 6. Same as Fig. 3, except for the average from 21 July 00:00 to 22 July 00:00 UTC

ulated precipitation upon the convective faction in the GF scheme. In particular, the comparison between Fig. 10a and Fig. 10b shows that as the spatial resolution transitions from 60km to 3km over the northern China, the convective precipitation significantly decreases while the resolved precipitation increases. The increasing resolved precipitation compensates smoothly decreasing parameterized precipitation over the area of mesh refinement, which means that the GF scheme accomplishes the remarkable scale-aware performance, enabling a continuous adjustment of the cloud mass flux based on the convective updraft fraction.

4.2 Spatial and Temporal Variation

Fig. 11 shows the meridional precipitation propagation over Henan province during the event. The CMA observation and the ERA5 reanalysis data show that the position of the rain belt moved northward from near 33°N on 19 July 00:00 UTC to 37°N on 22 July 00:00 UTC, with three peak periods of maximum precipitation intensity reaching its strongest point at

https://doi.org/10.5194/gmd-2023-193
Preprint. Discussion started: 5 October 2023

Geoscientific Model Development
Discussions

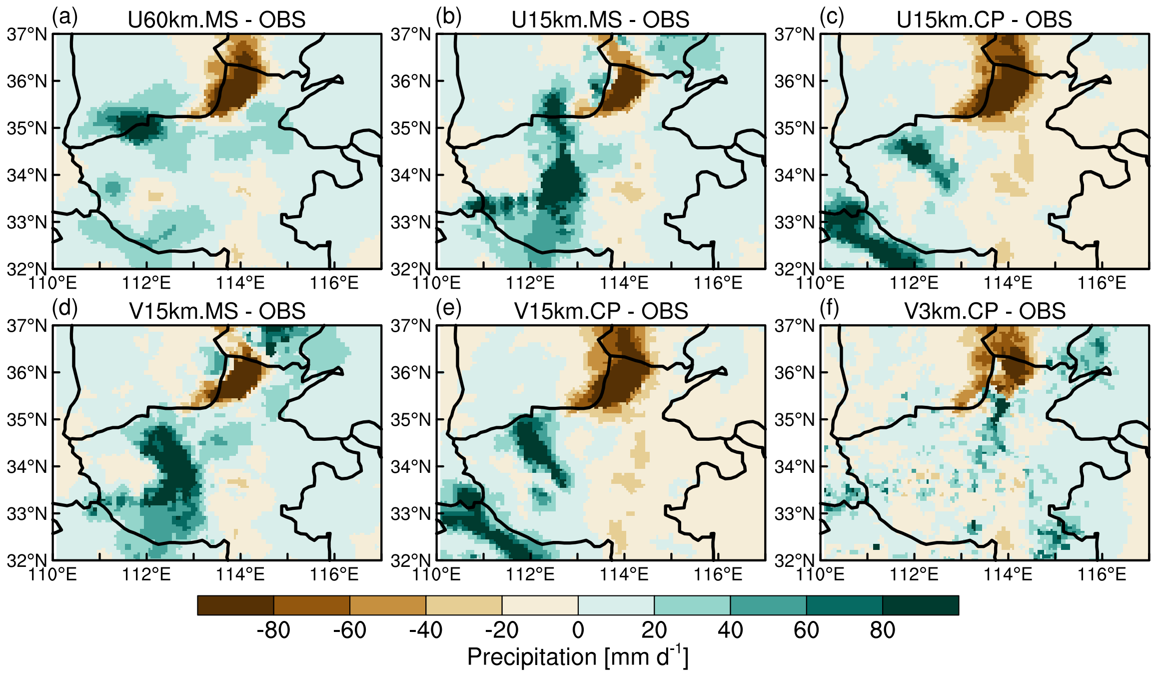

Figure 7. Same as Fig. 4, except for the average from 21 July 00:00 to 22 July 00:00 UTC

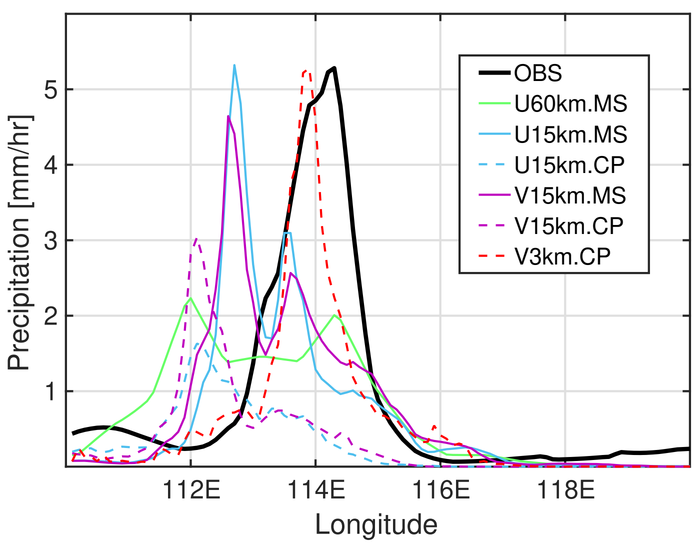

Figure 8. Same as Fig. 5, except for the average from 21 July 00:00 to 22 July 00:00 UTC

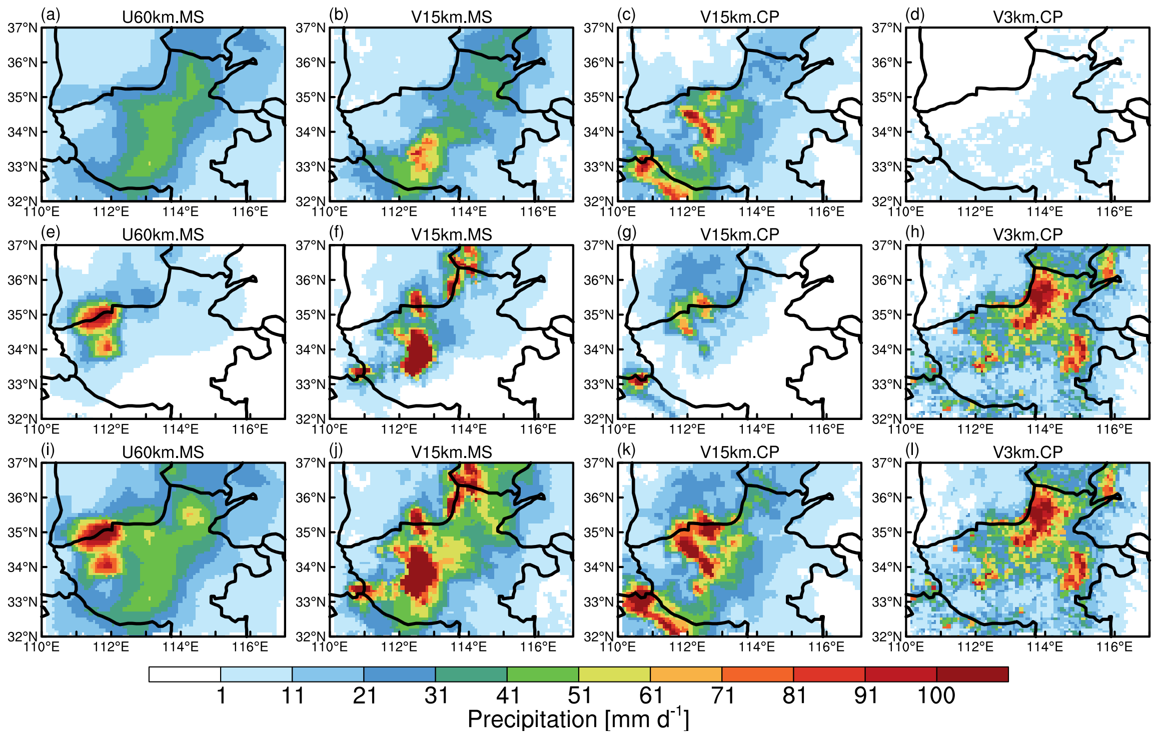

Figure 9. Spatial distribution of parameterized (upper four panels), resolved (medium four panels), and total (lower four panels) precipitation averaged from 20 July 00:00 to 22 July 00:00 UTC over Henan province from the simulations with resolutions of 60, 15, and 3km, respectively.

00:00 UTC on July 21. Fig. 11c-h present the model simulations with various resolutions and parameterization schemes. All simulations effectively predicted the northward movement of the precipitation pattern. The performance of the CP parameterization scheme suite and the MS parameterization scheme suite at 15km is comparable. However, none of the simulations with CP parameterization scheme suite were able to effectively predict the 3rd peak, except for the V3km.CP simulation. The U60km.MS simulation effectively captured the trend of northward movement of the precipitation location, but its simulated precipitation center at the 3rd peak is placed further north compared to the observation. In addition, the performances of the 15km variable-resolution and quasi-uniform mesh are equivalent to each other with the same parameterization scheme suite. Among all simulations, V3km.CP simulation is closest to observations, as it effectively captures the three peaks and their timings are in the best agreement with observations. Moreover, the precipitation intensity simulated by V3km.CP is closest to observations.

In order to further evaluate the simulation performance of the rainfall location and intensity, we explore further by examining the simulated zonal propagation of rainfall over the Henan province from 20 July 00:00 to 22 July 00:00 UTC (Fig. 12). The precipitation mainly occurred at 113°E and there was a tendency for the precipitation to move eastward over time. Similarly,

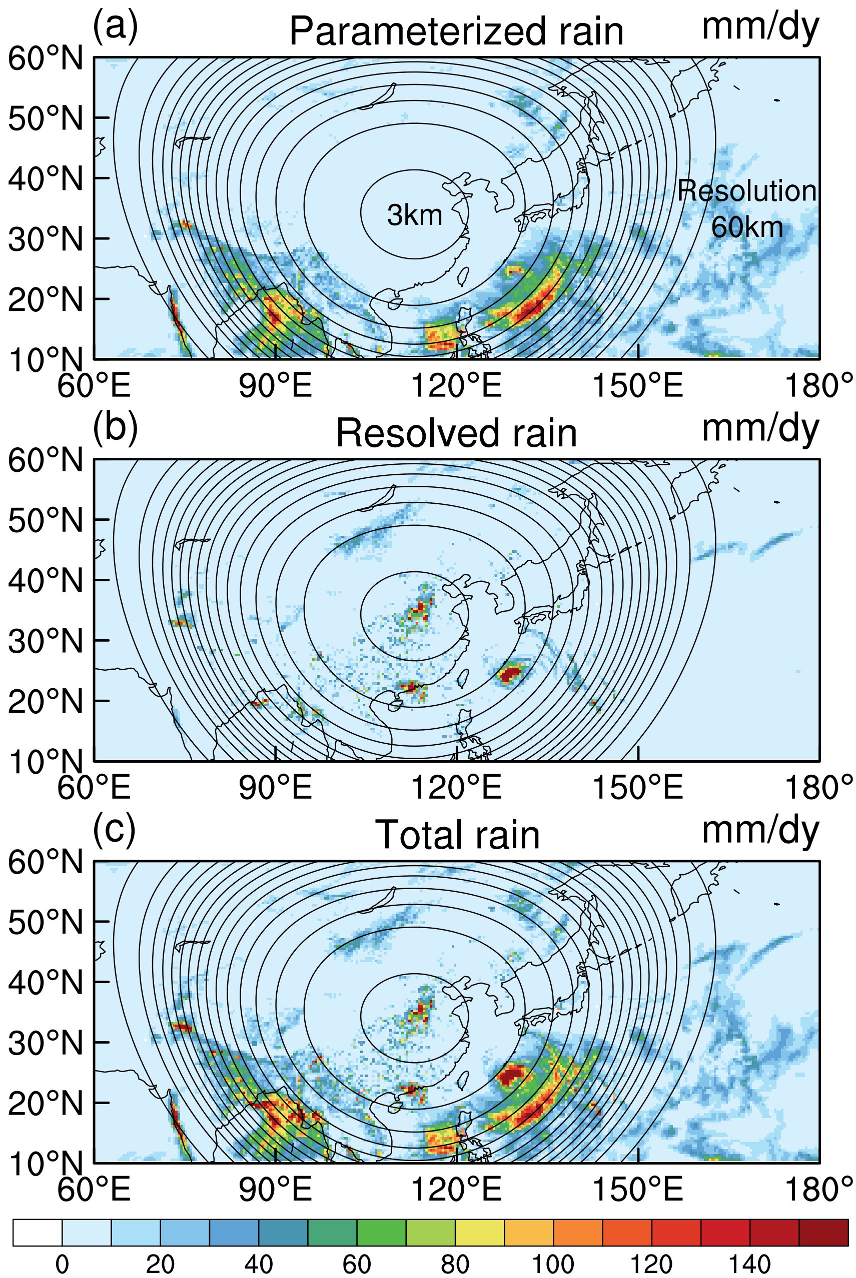

Figure 10. Spatial distribution of averaged parameterized, resolved, and total precipitation from 20 July 00:00 to 22 July 00:00 UTC from the V3km.CP simulation. The solid black line represents the grid resolution from 60km to 3km by 4km, and the label "3km"("60km") in the Fig. 10a denotes a horizontal resolution of 3km(60km) within the specified region.

https://doi.org/10.5194/gmd-2023-193
Preprint. Discussion started: 5 October 2023

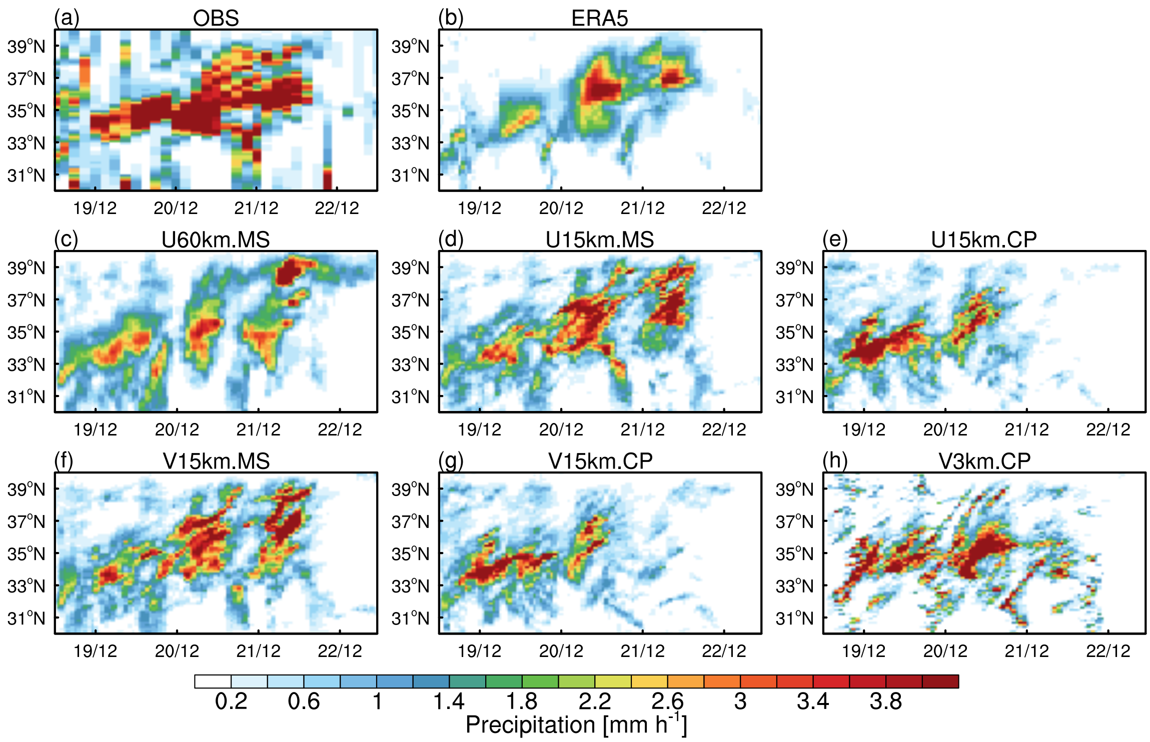

Figure 11. Time–Latitude cross section of precipitation over Henan province (30°N–40°N, 110°E–130°E) from the CMA station observations and the simulations with global uniform and variable-resolution with two parameterization scheme suites.

there were three distinct peak periods, which are consistent with the results discussed earlier. Once again, both V15km.CP and V15km.MS simulations exhibit comparable forecast performance. The precipitation forecasted by U60km.MS was biased towards the east, likely due to the coarse resolution. V3km.CP is closest to observation, in terms of both the predicted intensity and location, which is consistent with the results discussed above.

5 Conclusion and discussion

This pioneering study introduces a novel modeling approach to predicting a historic rainstorm occurred over Henan province, China, in July 2021 ("7.20" extreme precipitation) by utilizing a global variable-resolution non-hydrostatic model (MPAS-Atmosphere). A series of simulations have been done at both quasi-uniform (60km and 15km) and variable-resolution meshes (60-15km and 60-3km). For the 48-hour peak precipitation duration (07/20-07/22), the 60-3km variable-resolution simulation coupled with the scale-aware convection-permitting parameterization scheme suite stands out among all tested simulations as it reproduces this extreme precipitation event most accurately, in terms of both the intensity and location of the peak precipitation. At 15-km resolution, given the same parameterization schemes are selected, the 60-15km variable-resolution simulation

https://doi.org/10.5194/gmd-2023-193
Preprint. Discussion started: 5 October 2023

Geoscientific Model Development
Discussions

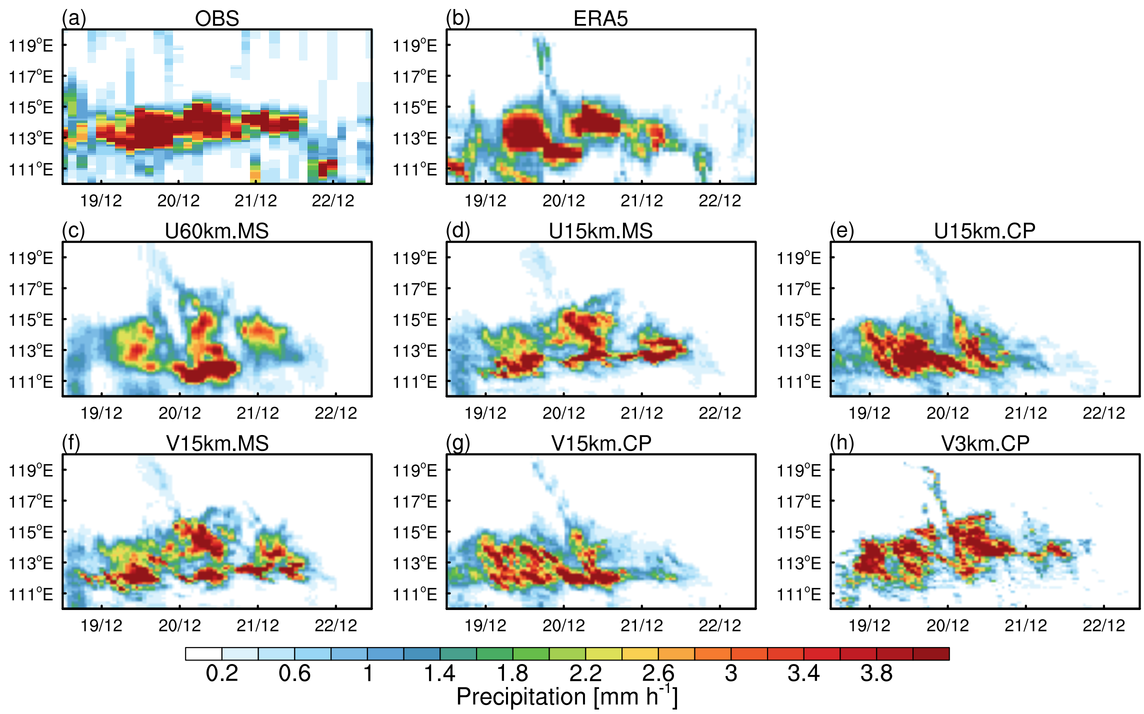

Figure 12. Time–longitude cross section of precipitation averaged over Henan province (30–40°N, 110–130°E) from the CMA station observations and the simulations with global uniform and variable-resolution with two schemes.

achieves comparable forecasting skills as the 15-km quasi-uniform simulation, but with the former being performed at a much reduced computing cost. In addition, we further compared two sets of built-in physical parameterization schemes, namely, the mesoscale suite and scale-aware convection-permitting suite, at quasi-uniform and variable-resolution mesh of 15 km respectively. We found that the default mesoscale suite generally outperforms the convection-permitting suite at 15-km resolution as both 15-km quasi-uniform and 60-15km variable-resolution simulations coupled with convection-permitting parameterization scheme suite missed the 3rd peak of the extreme precipitation event in contrast to simulations with mesoscale parameterization scheme suite. This implies that, when the resolution of the refined region is coarser than the cloud-resolving scale, the convection-permitting parameterization scheme suite does not necessarily work better than the default mesoscale suite, but once the refined mesh is close to the cloud-resolving scale, the convection-permitting suite becomes scale aware such that it can intelligently distinguish the convective precipitation and grid-scale precipitation, respectively. Hence, it is essential to match parameterization schemes with the grid resolution for optimal compatibility. Furthermore, through this study, we also found that the large-scale wind field plays a vital role in affecting the simulated extreme precipitation event since it largely influences the transport of the water vapor flux thereby altering the prediction of the precise peak precipitation location. Consequently, the latent heat release from the simulated peak precipitation would further feed back to the large-scale wind field such that the impact of the wind field upon the simulated peak precipitation is amplified.

Geoscientific Model Development Discussions

Xu et al. (2023) used WRF with one-way nesting in simulating this same "7.20" extreme precipitation event, by setting the resolution of the outer domain at 20 km and inner domain at 4 km, respectively. They found that their simulations with GF convection scheme generate large bias from the observed precipitation field, whereas our global 60-3km variable-resolution simulation with the same GF convection scheme gives much improved prediction of the extreme precipitation location as well as intensity. This implies that the seamless mesh transition of the global variable-resolution model is superior in simulating the extreme precipitation event. In addition, Xu et al. (2023) found that the misrepresented large-scale circulation in the outer domain, due to the excessive latent heat simulated from the flawed convective parameterization scheme, could substantially impact the simulated peak precipitation over the inner domain. This is consistent with our results as we found that the large-scale wind field predominately influences the simulated peak precipitation in our MPAS simulations as well.

Moreover, in this study, we demonstrate that in the high-resolution simulation (3km), the total precipitation is primarily contributed by grid-scale precipitation, whereas in the low-resolution simulation (60km, 15km), the total precipitation is mainly influenced by subgrid-scale precipitation, which is also found by previous studies (Fowler et al., 2016; Zhao et al., 2019). An evident characteristic is the smooth transition of grid-scale precipitation from the low-resolution region to the high-resolution region, which implies that the GF convective parameterization scheme is responsive to changes in resolution and promptly adjusts accordingly. These findings suggest that appropriate parameterization schemes need to be selected for different regions according to their respective grid scales. Furthermore, we emphasize the importance of considering the subgrid scale processes in precipitation simulations, as they play a significant role in the total precipitation, especially for simulations in refined areas.

This study found the global 60km-3km variable-resolution MPAS simulation coupled with scale-aware convection-permitting parameterization scheme suite outperforms alternative simulations, which is consistent with the previous studies (Zhao et al., 2019; Skamarock et al., 2018; Feng et al., 2018; Prein et al., 2015). In addition, the resolved lower boundary forcings such as topography and surface heterogeneity exert significant influence on regional precipitation simulations, signifying that the prediction of extreme precipitation events remains critical (Sakaguchi et al., 2015). Endeavors aimed at enhancing the scale-aware function of convective parameterization may yield further advancements in the future (Gao et al., 2017; Hagos et al., 2013; Skamarock et al., 2012). Further study is needed to investigate more quantitatively the sensitivity of the intensity and location of simulated extreme precipitation to the scaling factor in convection-permitting parameterization suite.

Code and data availability. The model (MPAS v7.3) used in this study can be downloaded from https://mpas-dev.github.io/. The global meshes generated for the experiments can be downloaded from https://mpas-dev.github.io/atmosphere/atmosphere_meshes.html. Hourly surface observation data used in this study can be downloaded from https://data.cma.cn/. Hourly precipitation data from the European Centre for Medium-Range Weather Forecasts (ECMWF) Reanalysis can be downloaded from https://cds.climate.copernicus.eu/cdsapp#!/home.

Author contributions. LD and ZL designed the study and the experiments. LD, ZL, HY, DM, and XQ analyzed the simulations. XL prepared and analyzed the observations. ZL, DL, and YW performed simulations and created the figures. All authors contributed to writing or discussing the manuscript.

Competing interests. The contact author has declared that none of the authors has any competing interests.

Acknowledgements. The authors thank European Centre for Medium-Range Weather Forecasts for providing datasets/models etc. All computations of this work were done at the Center for Computational Science and Engineering at Southern University of Science and Technology and we appreciate the high-quality service provided by the staff of this center. This work was supported in part by grants from the National Natural Science Foundation of China (Grant No. 41975060) and Shenzhen Science and Technology Program (Grant No. JCYJ20190809163007701 and JCY20200925160922002).

References

Arakawa, A., Jung, J.-H., and Wu, C.-M.: Toward unification of the multiscale modeling of the atmosphere, Atmospheric Chemistry and Physics, 11, 3731–3742, 2011.

Bechtold, P., Chaboureau, J.-P., Beljaars, A., Betts, A., Köhler, M., Miller, M., and Redelsperger, J.-L.: The simulation of the diurnal cycle of convective precipitation over land in a global model, Quarterly Journal of the Royal Meteorological Society: A journal of the atmospheric sciences, applied meteorology and physical oceanography, 130, 3119–3137, 2004.

Bechtold, P., Köhler, M., Jung, T., Doblas-Reyes, F., Leutbecher, M., Rodwell, M. J., Vitart, F., and Balsamo, G.: Advances in simulating atmospheric variability with the ECMWF model: From synoptic to decadal time-scales, Quarterly Journal of the Royal Meteorological Society: A journal of the atmospheric sciences, applied meteorology and physical oceanography, 134, 1337–1351, 2008.

Bechtold, P., Semane, N., Lopez, P., Chaboureau, J.-P., Beljaars, A., and Bormann, N.: Representing equilibrium and nonequilibrium convection in large-scale models, Journal of the Atmospheric Sciences, 71, 734–753, 2014.

Chen, F. and Dudhia, J.: Coupling an advanced land surface–hydrology model with the Penn State–NCAR MM5 modeling system. Part I: Model implementation and sensitivity, Monthly weather review, 129, 569–585, 2001.

Chen, F., Yuan, H., Sun, R., and Yang, C.: Streamflow simulations using error correction ensembles of satellite rainfall products over the Huaihe river basin, Journal of Hydrology, 589, 125 179, 2020.

Cheng, Y., Hui, P., Liu, D., Fang, J., Wang, S., Wang, S., and Tang, J.: MPAS-A Variable-Resolution Simulations for Summer Monsoon Over China: Comparison Between Global and Regional Configuration, Journal of Geophysical Research: Atmospheres, 128, e2022JD037 541, 2023.

Davis, C. A., Ahijevych, D. A., Wang, W., and Skamarock, W. C.: Evaluating medium-range tropical cyclone forecasts in uniform-and variable-resolution global models, Monthly Weather Review, 144, 4141–4160, 2016.

Ding, Y. and Johnny CL, C.: The East Asian summer monsoon: an overview, Meteorology and Atmospheric Physics, 89, 117–142, 2005.

Ding, Y., Wang, Z., and Sun, Y.: Inter-decadal variation of the summer precipitation in East China and its association with decreasing Asian summer monsoon. Part I: Observed evidences, International Journal of Climatology: A Journal of the Royal Meteorological Society, 28, 1139–1161, 2008.

Ding, Y., Liu, Y., and Hu, Z.-Z.: The record-breaking mei-yu in 2020 and associated atmospheric circulation and tropical SST anomalies, Advances in Atmospheric Sciences, 38, 1980–1993, 2021.

Du, Y. and Chen, G.: Heavy rainfall associated with double low-level jets over southern China. Part II: Convection initiation, Monthly Weather Review, 147, 543–565, 2019.

Feng, Z., Leung, L. R., Houze Jr, R. A., Hagos, S., Hardin, J., Yang, Q., Han, B., and Fan, J.: Structure and evolution of mesoscale convective systems: Sensitivity to cloud microphysics in convection-permitting simulations over the United States, Journal of Advances in Modeling Earth Systems, 10, 1470–1494, 2018.

Fowler, L. D., Skamarock, W. C., Grell, G. A., Freitas, S. R., and Duda, M. G.: Analyzing the Grell–Freitas convection scheme from hydrostatic to nonhydrostatic scales within a global model, Monthly Weather Review, 144, 2285–2306, 2016.

Gao, Y., Leung, L. R., Zhao, C., and Hagos, S.: Sensitivity of US summer precipitation to model resolution and convective parameterizations across gray zone resolutions, Journal of Geophysical Research: Atmospheres, 122, 2714–2733, 2017.

Grell, G. A. and Dévényi, D.: A generalized approach to parameterizing convection combining ensemble and data assimilation techniques, Geophysical Research Letters, 29, 38–1, 2002.

Grell, G. A. and Freitas, S. R.: A scale and aerosol aware stochastic convective parameterization for weather and air quality modeling, Atmospheric Chemistry and Physics, 14, 5233–5250, 2014.

Hagos, S., Leung, R., Rauscher, S. A., and Ringler, T.: Error characteristics of two grid refinement approaches in aquaplanet simulations: MPAS-A and WRF, Monthly Weather Review, 141, 3022–3036, 2013.

Hong, S.-Y.: A new stable boundary-layer mixing scheme and its impact on the simulated East Asian summer monsoon, Quarterly Journal of the Royal Meteorological Society, 136, 1481–1496, 2010.

Hong, S.-Y. and Lim, J.-O. J.: The WRF single-moment 6-class microphysics scheme (WSM6), Asia-Pacific Journal of Atmospheric Sciences, 42, 129–151, 2006.

Hong, S.-Y., Noh, Y., and Dudhia, J.: A new vertical diffusion package with an explicit treatment of entrainment processes, Monthly weather review, 134, 2318–2341, 2006.

Houze Jr, R. A.: Mesoscale convective systems, Reviews of Geophysics, 42, 2004.

Iacono, M. J., Mlawer, E. J., Clough, S. A., and Morcrette, J.-J.: Impact of an improved longwave radiation model, RRTM, on the energy budget and thermodynamic properties of the NCAR community climate model, CCM3, Journal of Geophysical Research: Atmospheres, 105, 14 873–14 890, 2000.

Jinfang, Y., Haodong, G., Liang, X., Miao, Y., Jisong, S., Yanxin, X., Feng, L., and Chong, W.: A possible dynamic mechanism for rapid production of the extreme hourly rainfall in Zhengzhou City on 20 July 2021, Journal of Meteorological Research, 36, 6–25, 2021.

Klemp, J. B.: A terrain-following coordinate with smoothed coordinate surfaces, Monthly weather review, 139, 2163–2169, 2011.

Klemp, J. B., Skamarock, W. C., and Dudhia, J.: Conservative split-explicit time integration methods for the compressible nonhydrostatic equations, Monthly Weather Review, 135, 2897–2913, 2007.

Li, Z., Lau, W.-M., Ramanathan, V., Wu, G., Ding, Y., Manoj, M., Liu, J., Qian, Y., Li, J., Zhou, T., et al.: Aerosol and monsoon climate interactions over Asia, Reviews of Geophysics, 54, 866–929, 2016.

Liang, Y., Yang, B., Wang, M., Tang, J., Sakaguchi, K., Leung, L. R., and Xu, X.: Multiscale Simulation of Precipitation Over East Asia by Variable Resolution CAM-MPAS, Journal of Advances in Modeling Earth Systems, 13, e2021MS002 656, 2021.

Liu, B., Yan, Y., Zhu, C., Ma, S., and Li, J.: Record-breaking Meiyu rainfall around the Yangtze River in 2020 regulated by the subseasonal phase transition of the North Atlantic Oscillation, Geophysical Research Letters, 47, e2020GL090 342, 2020.

Lonfat, M., Marks Jr, F. D., and Chen, S. S.: Precipitation distribution in tropical cyclones using the Tropical Rainfall Measuring Mission (TRMM) Microwave Imager: A global perspective, Monthly Weather Review, 132, 1645–1660, 2004.

Nakanishi, M. and Niino, H.: An improved Mellor–Yamada level-3 model: Its numerical stability and application to a regional prediction of advection fog, Boundary-Layer Meteorology, 119, 397–407, 2006.

Nakanishi, M. and Niino, H.: Development of an improved turbulence closure model for the atmospheric boundary layer, Journal of the Meteorological Society of Japan. Ser. II, 87, 895–912, 2009.

Nie, Y. and Sun, J.: Moisture sources and transport for extreme precipitation over Henan in July 2021, Geophysical Research Letters, 49, e2021GL097 446, 2022.

Park, S.-H., Skamarock, W. C., Klemp, J. B., Fowler, L. D., and Duda, M. G.: Evaluation of global atmospheric solvers using extensions of the Jablonowski and Williamson baroclinic wave test case, Monthly Weather Review, 141, 3116–3129, 2013.

Prein, A. F., Langhans, W., Fosser, G., Ferrone, A., Ban, N., Goergen, K., Keller, M., Tölle, M., Gutjahr, O., Feser, F., et al.: A review on regional convection-permitting climate modeling: Demonstrations, prospects, and challenges, Reviews of geophysics, 53, 323–361, 2015.

Rauscher, S. A., Ringler, T. D., Skamarock, W. C., and Mirin, A. A.: Exploring a global multiresolution modeling approach using aquaplanet simulations, Journal of Climate, 26, 2432–2452, 2013.

Sakaguchi, K., Leung, L. R., Zhao, C., Yang, Q., Lu, J., Hagos, S., Rauscher, S. A., Dong, L., Ringler, T. D., and Lauritzen, P. H.: Exploring a multiresolution approach using AMIP simulations, Journal of Climate, 28, 5549–5574, 2015.

Skamarock, W. C. and Gassmann, A.: Conservative transport schemes for spherical geodesic grids: High-order flux operators for ODE-based time integration, Monthly Weather Review, 139, 2962–2975, 2011.

Skamarock, W. C. and Klemp, J. B.: A time-split nonhydrostatic atmospheric model for weather research and forecasting applications, Journal of computational physics, 227, 3465–3485, 2008.

Skamarock, W. C., Klemp, J. B., Duda, M. G., Fowler, L. D., Park, S.-H., and Ringler, T. D.: A multiscale nonhydrostatic atmospheric model using centroidal Voronoi tesselations and C-grid staggering, Monthly Weather Review, 140, 3090–3105, 2012.

Skamarock, W. C., Duda, M. G., Ha, S., and Park, S.-H.: Limited-area atmospheric modeling using an unstructured mesh, Monthly Weather Review, 146, 3445–3460, 2018.

Skamarock, W. C., Snyder, C., Klemp, J. B., and Park, S.-H.: Vertical resolution requirements in atmospheric simulation, Monthly Weather Review, 147, 2641–2656, 2019.

Sun, R., Yuan, H., and Yang, Y.: Using multiple satellite-gauge merged precipitation products ensemble for hydrologic uncertainty analysis over the Huaihe River basin, Journal of Hydrology, 566, 406–420, 2018.

Sun, W., Mu, X., Song, X., Wu, D., Cheng, A., and Qiu, B.: Changes in extreme temperature and precipitation events in the Loess Plateau (China) during 1960–2013 under global warming, Atmospheric Research, 168, 33–48, 2016.

Thompson, G. and Eidhammer, T.: A study of aerosol impacts on clouds and precipitation development in a large winter cyclone, Journal of the atmospheric sciences, 71, 3636–3658, 2014.

Thompson, G., Field, P. R., Rasmussen, R. M., and Hall, W. D.: Explicit forecasts of winter precipitation using an improved bulk microphysics scheme. Part II: Implementation of a new snow parameterization, Monthly Weather Review, 136, 5095–5115, 2008.

Tiedtke, M.: A comprehensive mass flux scheme for cumulus parameterization in large-scale models, Monthly weather review, 117, 1779–1800, 1989.

Wang, B., Xiang, B., and Lee, J.-Y.: Subtropical high predictability establishes a promising way for monsoon and tropical storm predictions, Proceedings of the National Academy of Sciences, 110, 2718–2722, 2013.

Wang, W.: Forecasting Convection with a "Scale-Aware" Tiedtke Cumulus Parameterization Scheme at Kilometer Scales, Weather and Forecasting, 37, 1491–1507, 2022.

Wicker, L. J. and Skamarock, W. C.: An Implicit–Explicit Vertical Transport Scheme for Convection-Allowing Models, Monthly Weather Review, 148, 3893–3910, 2020.

Xu, H., Duan, Y., and Xu, X.: Indirect Effects of Binary Typhoons on an Extreme Rainfall Event in Henan Province, China From 19 to 21 July 2021: 1. Ensemble-Based Analysis, Journal of Geophysical Research: Atmospheres, 127, e2021JD036 265, 2022.

Xu, M., Zhao, C., Gu, J., Feng, J., Hagos, S., Leung, L. R., Luo, Y., Guo, J., Li, R., and Fu, Y.: Convection-Permitting Hindcasting of Diurnal Variation of Mei-yu Rainfall Over East China With a Global Variable-Resolution Model, Journal of Geophysical Research: Atmospheres, 126, e2021JD034 823, 2021.

Xu, M., Zhao, C., Gu, J., Feng, J., Li, G., and Guo, J.: Appropriately representing convective heating is critical for predicting catastrophic heavy rainfall in 2021 in Henan Province of China, Environmental Research Communications, 2023.

https://doi.org/10.5194/gmd-2023-193
Preprint. Discussion started: 5 October 2023

Zhai, P., Zhang, X., Wan, H., and Pan, X.: Trends in total precipitation and frequency of daily precipitation extremes over China, Journal of climate, 18, 1096–1108, 2005.

Zhang, C., Wang, Y., and Hamilton, K.: Improved representation of boundary layer clouds over the southeast Pacific in ARW-WRF using a modified Tiedtke cumulus parameterization scheme, Monthly Weather Review, 139, 3489–3513, 2011.

Zhang, M. and Meng, Z.: Warm-sector heavy rainfall in southern China and its WRF simulation evaluation: A low-level-jet perspective, Monthly Weather Review, 147, 4461–4480, 2019.

Zhao, C., Leung, L. R., Park, S.-H., Hagos, S., Lu, J., Sakaguchi, K., Yoon, J., Harrop, B. E., Skamarock, W., and Duda, M. G.: Exploring the impacts of physics and resolution on aqua-planet simulations from a nonhydrostatic global variable-resolution modeling framework, Journal of Advances in Modeling Earth Systems, 8, 1751–1768, https://doi.org/https://doi.org/10.1002/2016MS000727, 2016.

Zhao, C., Xu, M., Wang, Y., Zhang, M., Guo, J., Hu, Z., Leung, L. R., Duda, M., and Skamarock, W.: Modeling extreme precipitation over East China with a global variable-resolution modeling framework (MPASv5.2): impacts of resolution and physics, Geoscientific Model Development, 12, 2707–2726, https://doi.org/10.5194/gmd-12-2707-2019, 2019.

Zheng, J. and Wang, C.: Influences of three oceans on record-breaking rainfall over the Yangtze River Valley in June 2020, Science China Earth Sciences, 64, 1607–1618, 2021.